Peer-reviewed version available at *Aerospace* **2018**, *5*, 11; doi:10.3390/aerospace5010011

Article

Experimental Implementation of a Passive Millimeter-Wave Fast Sequential Lobing Radiometric Seeker Sensor

Massimiliano Rossi [1,†,‡], Riccardo Maria Liberati[1,†,‡], Marco Frasca[1,†,‡], Mauro Angelini, [1,‡,*]

MBDA Italia S.p.A. Via Monte Flavio, 45 - 00131- Roma - Italy -

[1] massimiliano.rossi@mbda.it

[2] riccardo.liberati@mbda.it

[2] marco.frasca@mbda.it

[2] mauro.angelini@mbda.it

* Correspondence: massimiliano.rossi@mbda.it; Tel.: +39-06-87711

‡ These authors contributed equally to this work.

Abstract: The paper investigates the theory of operation of a passive millimeter-wave seeker sensor using fast electronic sequential-lobing technique and the experimental validation obtained through laboratory trials. The paper analyzes in detail the theoretical performance of a difference channel sensor and a pseudo-monopulse sensor deriving agile formulas for the estimation of target angular tracking accuracy and the subsequent experimental validation

Keywords: millimeter-wave; radiometer; sequential lobing

1. Introduction

Passive millimetre-wave sensors are widely used nowadays for different purposes. Principal civil applications of such sensors concern surveillance [1] [2] and navigation aid in adverse weather conditions [3] and concealed weapons and explosives detection in airports [4] [5]. Military applications span from surveillance through radiometric imaging to precision targeting [6]. While there is a lot of literature on Radars, very little (as far as the authors are concerned) seems to be available for this class of sensors that, while having similarities to classic radars, have significant differences in both operating principles and performances. The purpose of this paper is to examine in detail the target tracking accuracy of a four-beam millimetre-wave seeker sensor operating in W-band and its validation through experimental laboratory trials.

2. General Theory

Let a two-channel passive millimetre-wave radiometric seeker sensor be located in the origin of a Cartesian reference system so that the sensor's antenna boresight is coincident with the Z-axis and oriented as the the ordinary $\vec{k}$ versor. The antenna can be assumed to be a Cassegrain reflector with the feed organized as a "diamond" of four independent horns named "Up","Down","Left","Right" ("U/D","L/R" couples). Each horn generates a pencil beam squinted by a fixed angle with respect to the antenna boresight. Radiometric receivers are connected to U/D and L/R horns through dedicated millimetre-wave SPDTs driven by a control signal at audio frequency (several KHz). This allows the reception of the radiation coming to the four beams: the U/D couple with axes lying in the elevation plane and L/R one lying in the azimuthal plane as in Figure 1. Each couple operates independently from the other. The squint angle between U/D and L/R beams is such that 3dB beams contours can be assumed to be as Figure 2. A simplified system-level description of the receiver is depicted in Figure 3 where it is reported a parallel two-channel total power radiometric receiver. Each couple of antenna feeds is connected to a dedicated low loss millimeter-wave SPDT which output port is connected to a low noise amplifier, a band-pass filter and a detector. The output signal from the detector is injected into a synchronous demodulator driven by the same control signal used to control the SPDTs. The output signal is integrated and the corresponding signal processed in order to extract the information. As for first approximation it's possible to

Peer-reviewed version available at Aerospace 2018, 5, 11; doi:10.3390/aerospace5010011

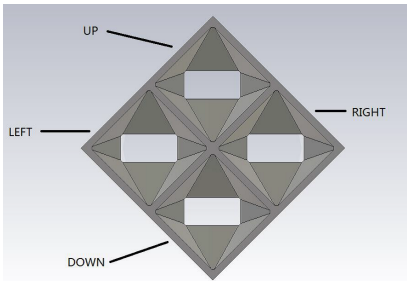

Figure 1. Diamond shaped Cassegrain feed

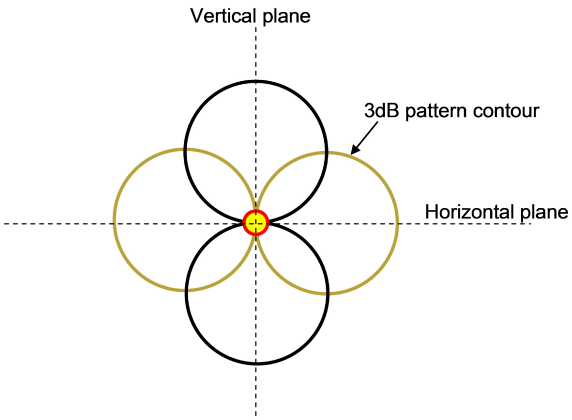

Figure 2. Radiometric seeker sensor 3dB contours

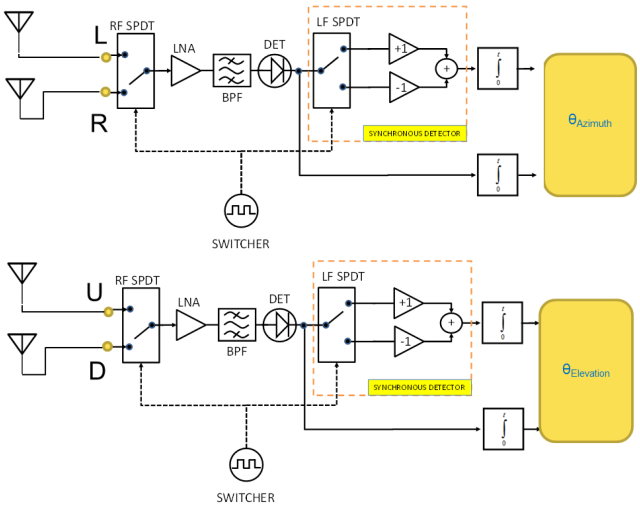

Figure 3. Simplified system-level schematic of a fast sequential-lobing radiometric seeker sensor

consider, for each beam, Gaussian power patterns as [7]

$$f(\vartheta,\phi) = G_o e^{-b\vartheta^2} \tag{1}$$

that depend only on the angle between the ordinary $\overrightarrow{k}$ versor and the generic positional versor $\overrightarrow{p}$. For such patterns, the constant b is [7]:

$$b = \frac{4\log(2)}{\vartheta_{3dB}^2} \tag{2}$$

Peer-reviewed version available at Aerospace 2018, 5, 11; doi:10.3390/aerospace5010011

where ϑ_{3dB} is the full 3dB angle of the beam in radiant. Now, let us consider a Gaussian beam which axis is represented by the versor $\overrightarrow{ax_o} = [\sin(\vartheta)\cos(\phi), \sin(\vartheta)\sin(\phi), \cos(\vartheta)]$. The angle ψ between a generic positional versor $\overrightarrow{p}$ and the axial versor $\overrightarrow{ax_o}$ is:

$$\psi = \cos^{-1}\left[\overrightarrow{ax_o} \cdot \overrightarrow{p}\right] \tag{3}$$

in fact, the angle ϑ inside (1) comes from:

$$\psi = \cos^{-1}\left([\sin(\vartheta)\cos(\phi), \sin(\vartheta)\sin(\phi), \cos(\vartheta)] \cdot [0,0,1]\right) = \cos^{-1}[\cos(\vartheta)] = \vartheta \tag{4}$$

more in general, if:

$$\overrightarrow{p} = [\sin(\vartheta_o)\cos(\phi_o), \sin(\vartheta_o)\sin(\phi_o), \cos(\vartheta_o)] \tag{5}$$

then:

$$\psi = \cos^{-1}\left[[\sin(\vartheta)\cos(\phi), \sin(\vartheta)\sin(\phi), \cos(\vartheta)] \cdot \overrightarrow{p}\right] \tag{6}$$

or

$$\psi = \cos^{-1}[\sin(\vartheta)\cos(\phi)\sin(\vartheta_o)\cos(\phi_o) + \sin(\vartheta)\sin(\phi)\sin(\vartheta_o)\sin(\phi_o) + \cos(\vartheta)\cos(\vartheta_o)] \tag{7}$$

now, if the position versor $\overrightarrow{p}$ lies on the YZ plane with the application point in the origin and oriented as $\phi_o = 0$, it follows that:

$$\psi_0(\vartheta, \phi, \vartheta_o) = \cos^{-1}[\sin(\vartheta)\cos(\phi)\sin(\vartheta_o) + \cos(\vartheta)\cos(\vartheta_o)] \tag{8}$$

$$\beta_o = \left(\cos^{-1}[\psi_0(\vartheta, \phi, \vartheta_o)]\right)^2 \tag{9}$$

$$f_{dx}(\vartheta, \phi) = G_o e^{-b\cdot\beta_0} \tag{10}$$

the same can be done for the antenna power pattern having the axis oriented such that $\phi_o = \pi$:

$$\psi_\pi(\vartheta, \phi, \vartheta_o) = \cos^{-1}[-\sin(\vartheta)\cos(\phi)\sin(\vartheta_o) + \cos(\vartheta)\cos(\vartheta_o)] \tag{11}$$

$$\beta_\pi = \left(\cos^{-1}[\psi_\pi(\vartheta, \phi, \vartheta_o)]\right)^2 \tag{12}$$

$$f_{sx}(\vartheta, \phi) = G_o e^{-b\cdot\beta_\pi} \tag{13}$$

in Figure 4 are reported for clarity, four squinted Gaussian beams with axes on XZ and YZ planes. The generic

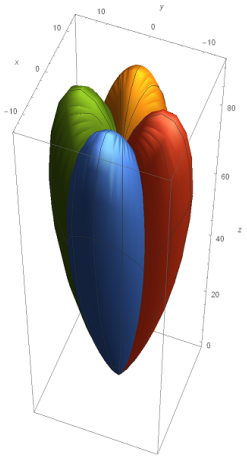

Figure 4. Squinted Gaussian power patterns

Peer-reviewed version available at Aerospace 2018, 5, 11; doi:10.3390/aerospace5010011

power pattern is a pencil-beam by hypothesis and the angle β is always small, so that the function $\psi(\vartheta, \phi, \vartheta_o) \cong 1$. This condition allows to approximate β by a Taylor series of the first order around one:

$$\left[\cos^{-1}(x)\right]^2 \cong 2 - 2x \tag{14}$$

substituting the (14) into the (13) follows that:

$$f_{dx}(\vartheta, \phi) = G_o e^{-b(2-2(\cos(\vartheta)\cos(\vartheta_o)+\cos[\phi]\sin(\vartheta)\sin(\vartheta_o)))} \tag{15}$$

the squint angle of the beams with respect to the Z axis, ϑ_o, is small (fractions of degree) so it is possible to approximate the (15) using Maclaurin series of the second order around zero in ϑ_o:

$$f_{dx}(\vartheta, \phi) \approx G_o e^{-2b+2b\cos(\vartheta)}]\left[1 + 2b\cos[\phi]\sin(\vartheta)\vartheta_o + b\left(-\cos(\vartheta) + 2b\cos(\phi)^2\sin(\vartheta)^2\right)\vartheta_o^2\right] \tag{16}$$

the same can be done for $f_{sx}(\vartheta, \phi)$. An antenna pattern requires that [8]:

$$\int_0^{2\pi}\int_0^{\pi} f(\vartheta, \phi)\sin(\vartheta)\, d\vartheta d\phi = 4\pi \tag{17}$$

solving the (17) using the (16) gives:

$$\frac{G_o\pi\left(1 - e^{-4b}\right)}{b} = 4\pi \tag{18}$$

that, with the constant b large enough [1] gives:

$$G_o \cong 4b \tag{19}$$

17 **3. Radiometric Delta Signals Calculation**

A basic geometry of the problem is depicted in Figure 5 where only the L/R beams are considered, for simplicity. It can be assumed the presence of a target with circular transverse area A_T on the Z axis at a distance R from the origin (and the antenna system). Such a target is seen under an angle of $2\Delta\vartheta_T$ radians by an observer in the origin. Each beam covers a different portion of the space and partially dwells the target as this

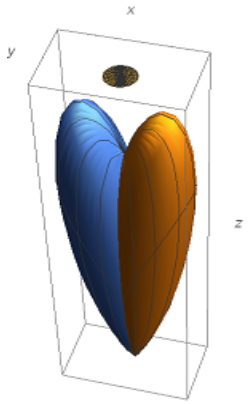

Figure 5. Target and L/R beams geometry

changes its angular coordinates. With reference to L/R beams (azimuthal plane), the corresponding antenna noise temperatures [9] can be put in the form :

$$TA_{f1} = \frac{1}{4\pi}\int_0^{2\pi}\int_0^{\Delta\vartheta_T}(T_{tgt}-T_{btgt})\cdot f_{dx}(\vartheta,\phi)\sin(\vartheta)\,d\vartheta d\phi + \frac{1}{4\pi}\int_0^{2\pi}\int_0^{\pi}T(\vartheta,\phi)\cdot f_{dx}(\vartheta,\phi)\sin(\vartheta)\,d\vartheta d\phi \quad (20)$$

$$TA_{f2} = \frac{1}{4\pi}\int_0^{2\pi}\int_0^{\Delta\vartheta_T}(T_{tgt}-T_{btgt})\cdot f_{sx}(\vartheta,\phi)\sin(\vartheta)\,d\vartheta d\phi + \frac{1}{4\pi}\int_0^{2\pi}\int_0^{\pi}T(\vartheta,\phi)\cdot f_{sx}(\vartheta,\phi)\sin(\vartheta)\,d\vartheta d\phi \quad (21)$$

T_{tgt}, T_{btgt} are the radiometric temperatures of the target and the background, hidden by the target itself. $T(\vartheta,\phi)$ is the radiometric temperature of the scenario except the target. As the angles between the axes of the antenna beams are small and each beam is highly directive, it can be assumed (as for approximation) that the radiometric temperature of the scenario,T_s, is the same for either beam. So:

$$TA_{f1} = \frac{1}{4\pi}\int_0^{2\pi}\int_0^{\Delta\vartheta_T}(T_{tgt}-T_{btgt})\cdot f_{dx}(\vartheta,\phi)\sin(\vartheta)\,d\vartheta d\phi + T_s = \frac{1}{4\pi}\int_0^{2\pi}\int_0^{\Delta\vartheta_T}\Delta T_T\cdot f_{dx}(\vartheta,\phi)\sin(\vartheta)\,d\vartheta d\phi + T_s \quad (22)$$

$$TA_{f2} = \frac{1}{4\pi}\int_0^{2\pi}\int_0^{\Delta\vartheta_T}(T_{tgt}-T_{btgt})\cdot f_{sx}(\vartheta,\phi)\sin(\vartheta)\,d\vartheta d\phi + T_s = \frac{1}{4\pi}\int_0^{2\pi}\int_0^{\Delta\vartheta_T}\Delta T_T\cdot f_{sx}(\vartheta,\phi)\sin(\vartheta)\,d\vartheta d\phi + T_s \quad (23)$$

where ΔT_T is the *radiometric contrast of the target*. The difference between the antenna noise temperatures $\Delta T_A = TA_{f1} - TA_{f2}$ *is the information where the contribution due the scenario is, ideally, minimized.* If the whole antenna is fixed and the angular coordinates of the target change, this produces effects onto the received signal. A change of the angular position of the target by an angle -β in the XZ plane corresponds to a rotation of the whole antenna by an angle β around the X axis with the target fixed. In fact, after some algebraic simplifications, we get:

$$\Delta(\vartheta,\phi,\beta) \cong -4bG_o\vartheta_o e^{2b(-1+\cos(\vartheta))}\left[-\beta\cos(\vartheta)+\cos(\phi)\sin(\vartheta)\left(-1+2b\cdot\beta\cos(\phi)\sin(\vartheta)\right)\right] \quad (24)$$

the difference between the antenna noise temperatures is:

$$\begin{aligned}\Delta(\vartheta,\phi,\beta) &= 4bG_o\vartheta_o e^{2b(1+\cos(\vartheta))}\left[\beta\cos(\vartheta)-\cos(\phi)\sin(\vartheta)\left(-1+2b\cdot\beta\cos(\phi)\sin(\vartheta)\right)\right]\\ \Delta T_A(\beta) &= \frac{\Delta T_T}{4\pi}\int_0^{2\pi}\int_0^{\Delta\vartheta_T}\Delta(\vartheta,\phi,\beta)\sin(\vartheta)\,d\vartheta d\phi\end{aligned} \quad (25)$$

so:

$$\Delta T_A(\beta) = G_o\cdot b\cdot\vartheta_o\cdot\beta\cdot\Delta T_T e^{2b(-1+\cos(\Delta\vartheta_T))}\sin(\Delta\vartheta_T)^2 \quad (26)$$

the (26) indicates that for small values of β (target close to the antenna boresight: tracking condition), the radiometric difference is a linear function of the angular displacement of the target over the plane of the beam axes. The maximum sensitivity is reached when the squint angle ϑ_o is such that:

$$\frac{\partial}{\partial\vartheta_o}\left(\frac{\partial}{\partial\vartheta}\left[f_{dx}(\vartheta,\phi)-f_{sx}(\vartheta,\phi)\right]\Big|_{\vartheta=0}\right)=0 \quad (27)$$

which corresponds to:

$$\vartheta_o \cong \frac{\vartheta_{3dB}}{\sqrt{8\log 2}} \cong 0.42\cdot\vartheta_{3dB} \quad (28)$$

so, it's possible to consider a squint angle of:

$$\vartheta_o = \frac{\vartheta_{3dB}}{2} \tag{29}$$

without introducing significant losses. As the (26) comes from approximations of the power patterns, the calculation of the radiometric delta has also been carried out numerically. The error introduced by the approximated method has been estimated deriving a corrective factor α, that is a function of the ratio between the apparent angle of the target $\Delta\vartheta_T$ and the full 3dB angle of the beams ϑ_{3dB}. The corrective factor α is reported in

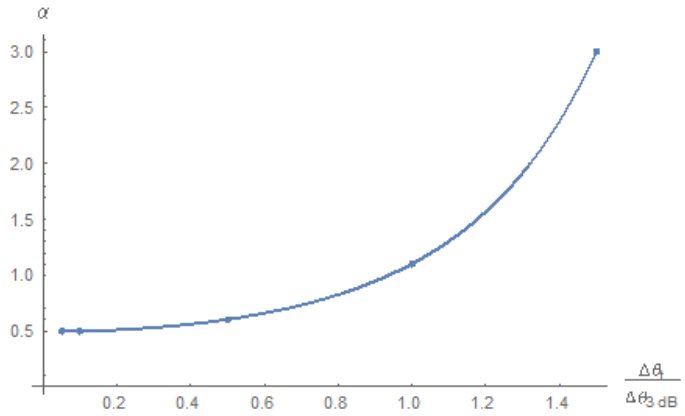

Figure 6. Corrective factor to be applied to the approximated formula

Figure 6 and very well approximated by:

$$\alpha \cong \frac{1}{2} e^{0.77 \frac{\Delta\vartheta_T^2}{\vartheta_{3dB}^2}} \tag{30}$$

so, the correct radiometric delta is:

$$\Delta T_A(\beta) = \frac{1}{2} b G_o \beta \vartheta_o \Delta T_T e^{0.77 \frac{\Delta\vartheta_T^2}{\vartheta_{3dB}^2} + 2b[-1+\cos(\Delta\vartheta_T)]} \sin^2(\Delta\vartheta_T) \tag{31}$$

if $\beta = x \cdot \vartheta_{3dB}$ after some algebraic manipulations and writing the target angular position in fractions of the 3-dB angle of the beams results:

$$\Delta T_A(x) = \Delta T_T [4\log(2)]^2 \left(\frac{\Delta\vartheta_T^2}{\vartheta_{3dB}^2}\right) e^{-2 \frac{\Delta\vartheta_T^2}{\vartheta_{3dB}^2} \cdot x} \quad \text{con} \; -\frac{1}{2} \le x \le \frac{1}{2} \tag{32}$$

a similar expression holds for the radiometric over the elevation plane. In Tab.1 are reported, for comparison, the radiometric deltas obtained numerically and with the approximated method, letting $\Delta T_T = 1$ $[K]$ for simplicity.

Preprints (www.preprints.org) | NOT PEER-REVIEWED | Posted: 23 November 2017 doi:10.20944/preprints201711.0155.v1

Peer-reviewed version available at Aerospace 2018, 5, 11; doi:10.3390/aerospace5010011

Table 1. Radiometric deltas extracted numerically (blu) and using the closed approximated formula (yellow) for different values of parameter x

x=0.2	x=0.4
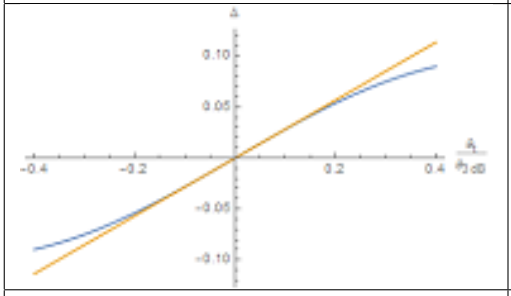	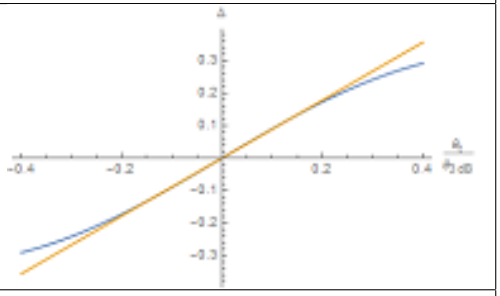
x=0.6	x=0.8
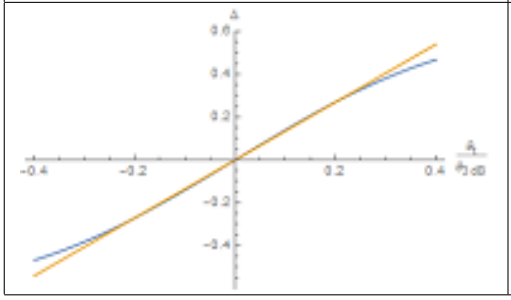	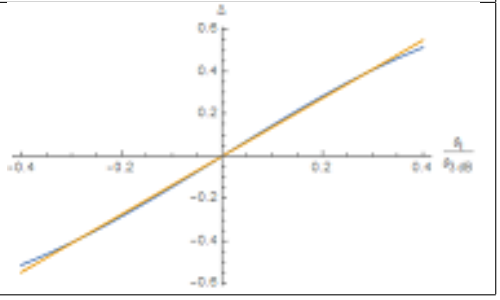

4. Angular accuracy estimation

L/R channel is connected to a radiometer who measures the antenna noise temperatures:

$$\begin{aligned} TA^*_{f1} &= TA_{f1} \pm \sigma_o \ [K] \\ TA^*_{f2} &= TA_{f2} \pm \sigma_o \end{aligned} \tag{33}$$

with uncertitude [10] $\sigma_o = \frac{\sqrt{2}T_0(F-1)}{\sqrt{B_{RF}\tau}}$ equal to the RMS value of the radiometric sensitivity of the receiver operating in time-sharing. As the useful signal is the difference between the noise temperatures reported in (26) the uncertitude of the difference is:

$$\Delta T^*_A = \Delta TA \pm \sigma_\Delta \tag{34}$$

with:

$$\sigma_\Delta = \sqrt{2}\sigma_o = \frac{2T_0(F-1)}{\sqrt{B_{RF}\tau}} \tag{35}$$

if:

$$K = \Delta T_T \left(\frac{\Delta \vartheta_T^2}{\vartheta_{3dB}^2} \right) e^{-2\frac{\Delta\vartheta_T^2}{\vartheta_{3dB}^2}} \tag{36}$$

than:

$$\Delta T^*_A(\beta) = K \left[4 \log(2) \right]^2 \frac{\beta}{\vartheta_{3dB}} \pm \sigma_\Delta \tag{37}$$

so, the estimated angle is:

$$\beta^* = \frac{\vartheta_{3dB}}{\left[4 \log(2) \right]^2 K} \Delta T^*_A(\beta) \pm \frac{\vartheta_{3dB}}{\left[4 \log(2) \right]^2 K} \sigma_\Delta \tag{38}$$

Peer-reviewed version available at Aerospace 2018, 5, 11; doi:10.3390/aerospace5010011

defining the radiometric SNR as:

$$SNR = \frac{\Delta T_T \left(\frac{\Delta\vartheta_T^2}{\vartheta_{3dB}^2}\right) e^{-2\frac{\Delta\vartheta_T^2}{\vartheta_{3dB}^2}}}{\sigma_\Delta} \tag{39}$$

the angular error is:

$$\sigma_\beta = \frac{1}{[4\log(2)]^2}\frac{\vartheta_{3dB}}{SNR} \cong \frac{\vartheta_{3dB}}{7.68}\frac{1}{SNR} \tag{40}$$

as:

$$\Delta\vartheta_T^2 \cong \frac{A_T}{\pi R^2} \tag{41}$$

considering the atmospheric attenuation neglibible, the (39) can be rewritten as:

$$SNR(R) = \Delta T_T \frac{A_T}{\pi R^2 \vartheta_{3dB}^2} e^{\left(-\frac{2A_T}{\pi R^2 \vartheta_{3dB}^2}\right)} \tag{42}$$

while:

$$\sigma_\beta = \frac{\vartheta_{3dB}}{7.68}\frac{\pi R^2 \vartheta_{3dB}^2 e^{\frac{2A_T}{\pi R^2 \vartheta_{3dB}^2}}}{\Delta T_T A_T} \tag{43}$$

the radiometric delta signal (32) could be normalized with respect to the "sum" signal in order to minimize the contribution due to the variation of target radiometric contrast on the angular estimation, as described later.

5. Estimated results

For a sensor operating at 94 GHz using state of the art millimetre-wave components, it is reasonable to assume [11] $\vartheta_{3dB} = 1\ [^\circ]$, $\sigma_\Delta \cong 150\ [mK]$, $\Delta T_T \cong 100\ [K]$ and a target with $A_T = 30\ [m^2]$. A SNR ≥8 $[dB]$ (P_d =0.9, P_{fa} =10^{-6}) ensures an angular error of ~0.35 mrad (~ 2/100 of degree) at a distance $R \sim 2$ Km, as reported in Figure 7 and Figure 8. The target is seen by the sensor as a point and this condition is implicit in (32). It

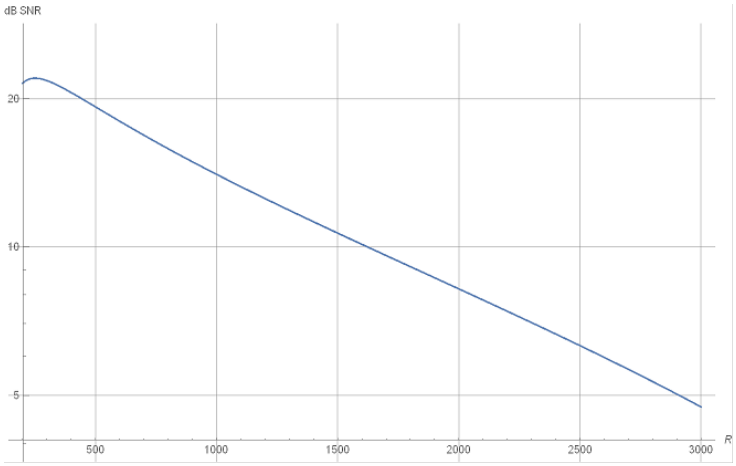

Figure 7. SNR as a function of the distance from the target

can be demonstrated that SNR has a maximum when $\frac{\Delta\vartheta_T^2}{\vartheta_{3dB}^2} = \frac{1}{2}$. It is easily perceivable that, when the target distance is small enough to make $TA_{f1} \cong TA_{f2}$ the SNR falls rapidly to zero while the angular error diverges. This condition however, corresponds to the final impact instants considering the high negative rate of variation of R. Looking at the behaviour of the normalized SNR expression of (39) as a function of the ratio $\gamma = \frac{\Delta\vartheta_T}{\vartheta_{3dB}}$,

Preprints (www.preprints.org) | NOT PEER-REVIEWED | Posted: 23 November 2017 doi:10.20944/preprints201711.0155.v1

Peer-reviewed version available at Aerospace 2018, 5, 11; doi:10.3390/aerospace5010011

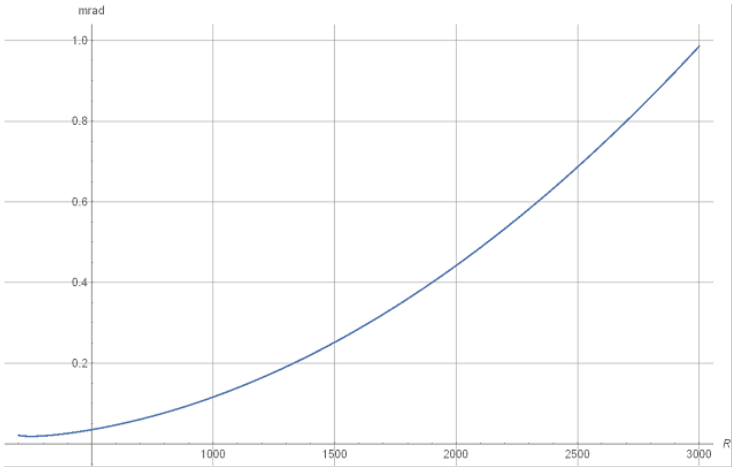

Figure 8. Angular error as a function of the distance from the target

depicted in Figure 9, it's possible to find out a range of γ values where, for the same target radiometric contrast, the SNR is high enough to allow target tracking with an acceptable angular error. A SNR ≥ 8 $[dB]$ requires:

$$\sqrt{\frac{-W\left(-2\cdot 10^{\frac{4}{5}}\frac{\sigma}{\Delta T_T}\right)}{2}} \leq \gamma \leq \sqrt{\frac{-W\left(-1,-2\cdot 10^{\frac{4}{5}}\frac{\sigma}{\Delta T_T}\right)}{2}} \tag{44}$$

where $W(x)$ is the Lambert function, σ the radiometric sensitivity and ΔT_T the target radiometric contrast. With the parameters already used before, it follows that: $\gamma \cong 0.098$ and $\gamma \cong 1.69$ that corresponds to:

$$105 \leq R \leq 1800 \text{ [m]} \tag{45}$$

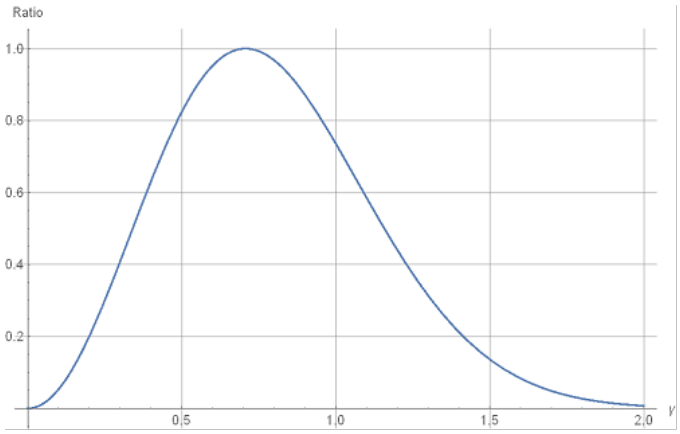

Figure 9. Behaviour of the normalized SNR as a function of γ (39)

6. Extension to a pseudo-monopulse architecture

The exclusive use of the "difference" signal makes the sensor dependent on the variations of the radiometric target contrast. For this purpose, it's possible to think to a pseudo-monopulse architecture where the difference signal is normalized to the "sum" signal. The correspondent analysis requires better approximations of the antenna noise temperatures. The use of normalized forms with respect the 3dB angle of $\Delta\vartheta_T$, ϑ_o and ϑ_t, has allowed the identification of suitable approximate expressions for L/R beams antenna noise temperatures through

numerical integration and parameters fitting. For target angular positions within half ϑ_{3dB} (in module), the noise temperatures have gaussian shapes with centers coincident with ϑ_o, but standard deviations dependent on the ratio $\frac{\vartheta_t}{\vartheta_{3dB}}$. Suitable expressions for the antenna noise temperatures of L/R beams are:

$$T_A \approx \Delta T_T \left(1 - e^{-4\log(2)\frac{\Delta\vartheta_T^2}{\vartheta_{3dB}^2}}\right) e^{-2\log(4)e^{-\log(4)\frac{\Delta\vartheta_T^2}{\vartheta_{3dB}^2}\left(\frac{\vartheta_t}{\vartheta_{3dB}}-\frac{\vartheta_o}{\vartheta_{3dB}}\right)^2}} + T_s \tag{46}$$

$$T_B \approx \Delta T_T \left(1 - e^{-4\log(2)\frac{\Delta\vartheta_T^2}{\vartheta_{3dB}^2}}\right) e^{-2\log(4)e^{-\log(4)\frac{\Delta\vartheta_T^2}{\vartheta_{3dB}^2}\left(\frac{\vartheta_t}{\vartheta_{3dB}}+\frac{\vartheta_o}{\vartheta_{3dB}}\right)^2}} + T_s \tag{47}$$

if the contribution due to T_s is small enough, it's possible to evaluate the ratio:

$$\frac{\Delta}{\Sigma} = \frac{T_A - T_B}{T_A + T_B} \tag{48}$$

if the target angular coordinate is close to the antenna axis, it's possible to write:

$$\frac{\Delta}{\Sigma} \cong 2\frac{2^{-2\frac{\Delta\vartheta_T^2}{\vartheta_{3dB}^2}}}{\vartheta_{3dB}}\log(4)\vartheta_t \tag{49}$$

the ratio is indipendent from the radiometric contrast of the target ΔT_T. The sensor works determining separately and independently the random variables:

$$X_1 = T_A^* - T_B^* \tag{50}$$

and :

$$Y_1 = T_A^* + T_B^* \tag{51}$$

the estimation of the angular coordinate of the target is done using a new random variable:

$$Z = \frac{X_1}{Y_1}$$

for the physics of the device, it can be demonstrated [10] that:

1. $X_1$is a gaussian random variable with expected value $\mu_1 = T_A - T_B$ and variance $\sigma^2 = \sigma_A^2 + \sigma_B^2$
2. $Y_1$is a gaussian random variable with expected value $\mu_1 = T_A + T_B$ and variance $\sigma^2 = \sigma_A^2 + \sigma_B^2$

so, T_A^* and T_B^* can be assumed to be uncorrelated and with the same variance σ^2. The standard deviation of Z is [12]:

$$\sigma_Z \cong \left|\frac{\mu_1}{\mu_2}\right| \sigma \sqrt{\left(\frac{1}{\mu_1^2} + \frac{1}{\mu_2^2}\right)} \tag{52}$$

but $\mu_1 \ll \mu_2$, so:

$$\sigma_Z \cong \left|\frac{1}{\mu_2}\right| \sigma \tag{53}$$

evaluating the "sum" signal around the origin:

$$\sigma_Z \cong \left|\frac{1}{\mu_2}\right| \sigma \cong \frac{2^{-1+2\frac{\Delta\vartheta_T^2}{\vartheta_{3dB}^2}}}{\Delta T_T \left(1 - e^{-4\log(2)\frac{\Delta\vartheta_T^2}{\vartheta_{3dB}^2}}\right)} \sigma \tag{54}$$

Peer-reviewed version available at Aerospace 2018, 5, 11; doi:10.3390/aerospace5010011

defining the "sum" channel SNR as:

$$SNR_{\Sigma} = \frac{1}{\sigma} \frac{\Delta T_T \left(1 - e^{-4\log(2)\frac{\Delta\vartheta_T^2}{\vartheta_{3dB}^2}} \right)}{2^{-1+2\frac{\Delta\vartheta_T^2}{\vartheta_{3dB}^2}}} \tag{55}$$

then:

$$\sigma_Z \cong \frac{1}{SNR_{\Sigma}} \tag{56}$$

the angular position of the target is tied with the ratio $\frac{\Delta}{\Sigma}$:

$$\vartheta_t = \frac{\vartheta_{3dB}}{2^{1-2\frac{\Delta\vartheta_T^2}{\vartheta_{3dB}^2}\log(4)}} \frac{\Delta}{\Sigma} \tag{57}$$

so, the RMS angular error is:

$$\sigma_{\vartheta_t} = \frac{1}{2\log(4)} \frac{1}{SNR_{\Sigma}} e^{2\frac{\Delta\vartheta_T^2}{\vartheta_{3dB}^2}} \vartheta_{3dB} \tag{58}$$

defining the slope of the difference channel normalized to the maximum value as:

$$K_m = 2^{-2\frac{\Delta\vartheta_T^2}{\vartheta_{3dB}^2}} \tag{59}$$

than, the angular error is:

$$\sigma_{\vartheta_t} \cong \frac{\vartheta_{3dB}}{2.77 K_m} \frac{1}{SNR_{\Sigma}} \tag{60}$$

the parameter:

$$\alpha = \frac{\Delta\vartheta_t}{\vartheta_{3dB}} \tag{61}$$

allows to easily represent the SNR ratios on the sum and difference channels and the angular error. Assuming, as done before, a radiometric contrast of $100[K]$ and a sensor sensitivity of $150[mK]$, the theoretical angular error is reported in Figure 10.

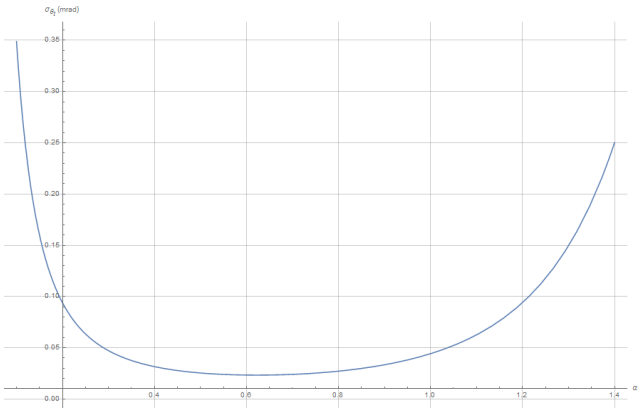

Figure 10. Angular error as a function of the ratio α

7. Experimental results

To validate the theory, a near zero emissivity chamber has been dedicated to the test of a custom W-band sensor. The laboratory walls have been completely covered by a 30 skin depths thick aluminium sheet in order

Peer-reviewed version available at Aerospace 2018, 5, 11; doi:10.3390/aerospace5010011

to obtain a "cold" room or a low emissivity environment, visible in Figure 11. In Figure 12 it is reported a

Figure 11. "Cold" laboratory chamber

simplified layout of the area with crooked walls in order to minimize successive reflections inside the volume. The sensor appears located on the left and two passive targets (Eccosorb ®panels) "Target 1" and "Target 2" with dimensions of 30 x 30 and 15 x 15 cm respectively are put on the right. The space between targets and "Target 2" dimensions have been selected in order to operate at Rayleigh limit at a distance of $\approx 4\ [m]$ from the seeker's antenna. Experimental trials have been conducted using a custom W-band sensor mounted over a

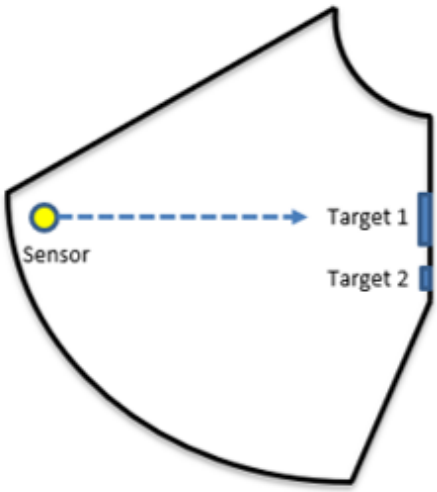

Figure 12. Laboratory layout

Pan-Tilt Unit-D100-EX screwed over a tripod, as depicted in Figure 13 in order to control the orientation of the sensor in near real time with high accuracy, instead of moving the targets. Laboratory tests were conducted only on the horizontal plane to minimize time and costs, while mechanical alignments and range measurements have been carried out using a laser range finder.

Peer-reviewed version available at Aerospace 2018, 5, 11; doi:10.3390/aerospace5010011

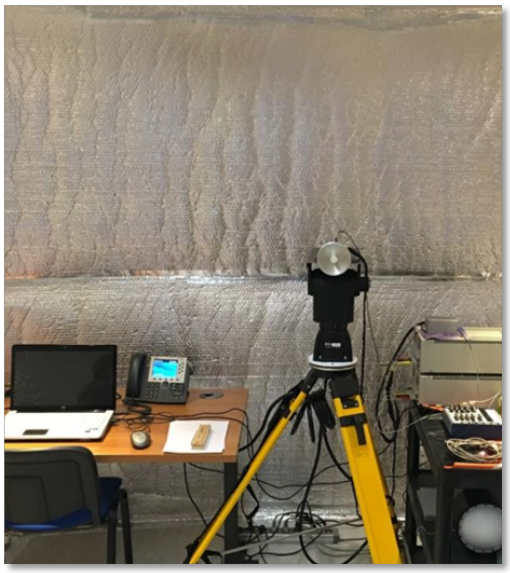

Figure 13. W-band sensor mounted on pan and tilt unit

A custom synchronous demodulator has been designed (Figure 14) and realized (Figure 15) in order to

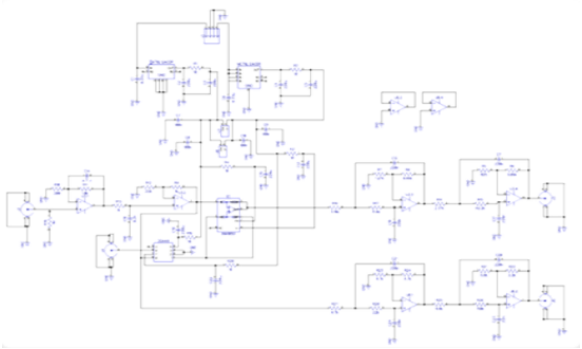

Figure 14. Synchronous demodulator scheme

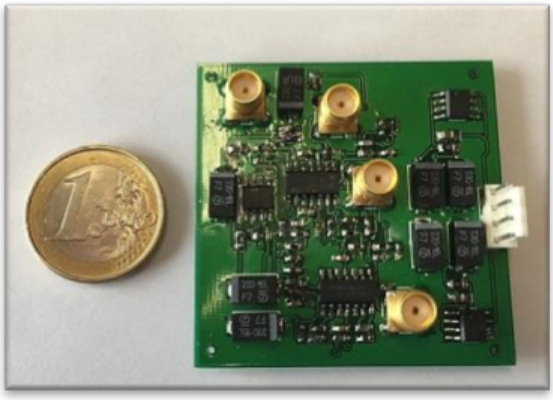

Figure 15. Actual synchronous demodulator

integrate and conveniently amplify the signal acquired by a National Instruments DAQ 6356. A preliminary test has been performed in order to estimate the available SNR inside the cold room, and obtain a rough target

Peer-reviewed version available at Aerospace 2018, 5, 11; doi:10.3390/aerospace5010011

position angular accuracy. For this purpose, a human target with known emissivity $\epsilon \approx 0.8$ has been located between "Target 1" and "Target 2", temporary covered by a metal sheet, and the system has been programmed to explore a 90° wide angular sector for 25 times. The target has been always detected as reported in Figure 16 allowing a rough position estimation $\theta \approx -4.2 \pm 0.2°$ with a SNR of about 10 dB, as reported in Figure 17.

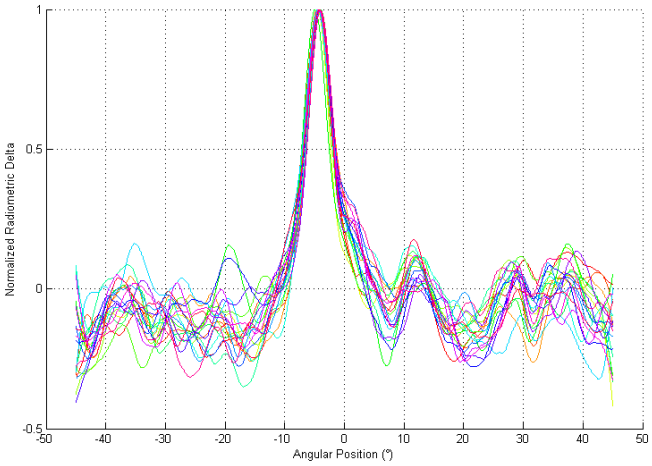

Figure 16. Human target radiometric pulses during search phase

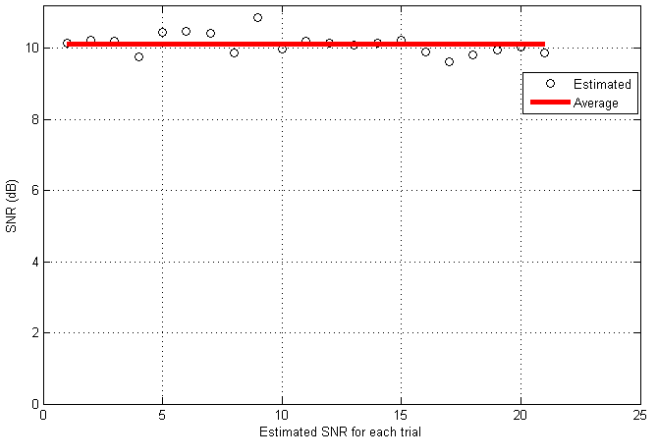

Figure 17. Estimated available SNR

Then the human target has been removed and the passive ones uncovered. So, a 90° wide angular sector has been scanned with an angular speed of 45°/s in order to search and identify the targets reported in Figure 18 obtaining two distinct radiometric pulses in considerable agreement with an integral model developed in Matlab ®and reported in Figure 19 in a normalized form.

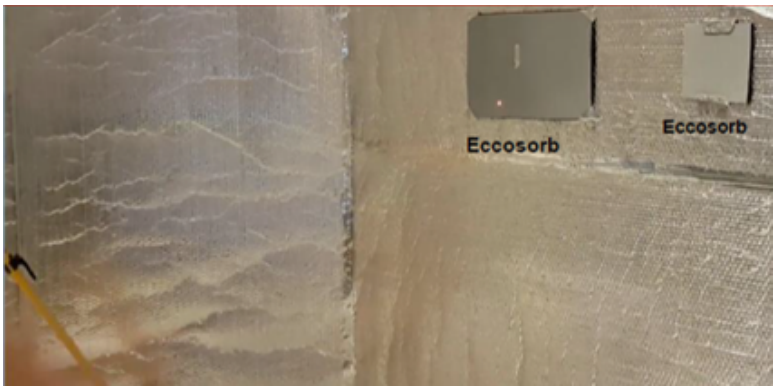

Figure 18. Passive "Target 1" and "Target 2"

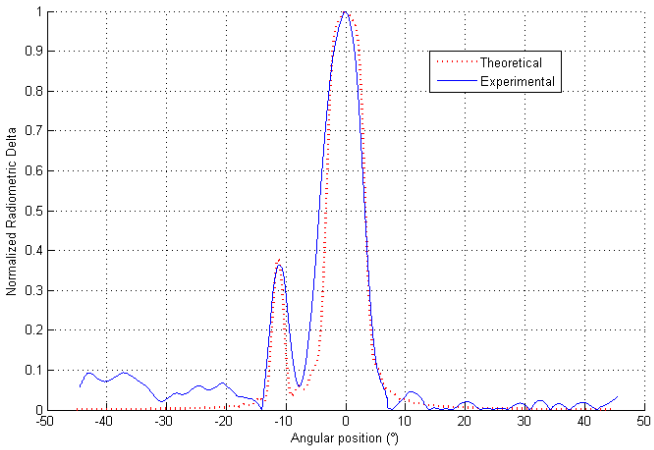

Figure 19. Radiometric pulses after search of two passive targets

Once acquired the potential targets, the computer has selected the biggest ("Target 1" hit by the laser spot in Figure 19) commanding the positioner to move to the correspondent position. A small angular sector scan has been performed around this position, in order to extract the "S" function reported in Figure 20. The difference between estimated theoretical angular accuracy $\sigma_\theta \approx 0.015\ [^\circ]$ and the experimental one $\sigma_\theta \approx 0.025\ [^\circ]$ appears to be very good, considering that thermal noise is not the only source of error.

Peer-reviewed version available at *Aerospace* **2018**, *5*, 11; doi:10.3390/aerospace5010011

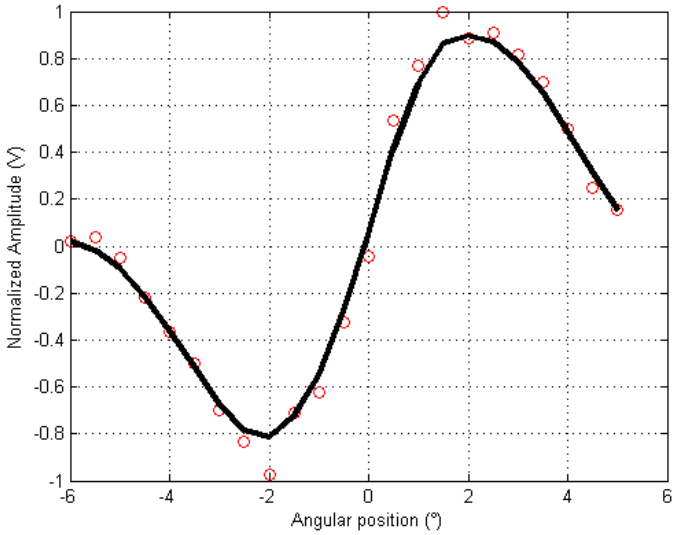

Figure 20. "S" function derived experimentally

8. Conclusions

Closed formulas for evaluating the angular tracking error of a four quadrant, double-channel millimetre-wave radiometric seeker sensor using fast electronic sequential-lobing technique, have been derived. Suitable closed formulas have been derived for a difference channel architecture and for a more accurate pseudo-monopulse one. The theory has been validated through experimental trials performed in a dedicated low-emisivity room using a custom W-band sensor. It has been demonstrated that a passive millimeter-wave sensor can provide guidance information as infrared ones and results indicate that the angular error is proportional to SNR^{-1} and not to $SNR^{-\frac{1}{2}}$ as in classical Radars [13] [14] [15]. Moreover, the pseudo-monopulse architecture needs only two indipendent receivers, but these are not required to be matched. During homing phase, when the distance of the target is relatively small, the technique can provide very accurate target tracking data.

References

1. Alimenti, F.; Bonafoni, S.; Leone, S.; Tasselli, G.; Basili, P.; Roselli, L.; Solbach, K. A Low-Cost Microwave Radiometer for the Detection of Fire in Forest Environments. *IEEE Trans. Geoscience and Remote Sensing* **2008**, *46*, 2632–2643.
2. Alimenti, F.; Roselli, L.; Bonafoni, S. Microwave Radiometers for Fire Detection in Trains: Theory and Feasibility Study †. Sensors, 2016.
3. Jacobs, E.L.; Furxhi, O. Target identification and navigation performance modeling of a passive millimeter wave imager. *Applied optics* **2010**, *49 19*, E94–105.
4. Nanzer, J. *Microwave and Millimeter-Wave Remote Sensing for Security Applications*; Artech House, 2012.
5. B. Kapilevich, B. Litvak, A.S.; Einat, M. Portable Passive Millimeter-Wave Sensor for Detecting Concealed Weapons and Explosives Hidden on a Human Body. *IEEE Sensors Journal* **2013**, *13*, 4224–4228.
6. James, D. *Radar Homing Guidance for Tactical Missiles*; Mac Millan Education LTD, 1986.
7. Jr., R.P.; Wilson, C. The VARR method, a Technique for Determining the Effective Power Patterns of Millimeter-Wave Radiometric Antennas. *BRL Report No.1322* **May 1966**.
8. Balanis, C.A. *Antenna Theory: Analysis and Design, 2nd Edition Ed.*; John Wiley and Sons Inc., 1997.
9. Otoshi, T.Y. *Noise Temperature Theory and Applications for Deep Space Communications Antenna Systems*; Artech House, 2008.
10. Racette, P.E.; Lang, R.H. Radiometer Design Analysis. 2008.
11. Skou N., L.V.D. *Microwave radiometer systems: design and analysis, 2nd*; Artech House, 2006.
12. Stuart, A.; Ord, K. *Kendall's Advanced Theory of Statistics*, 6th edition ed.; Vol. Volume 1, Arnold, 1998.

13. Levanon, N. *Radar Principles*; John Wiley and Sons Inc., 1988.
14. Barton, D.K.; Sherman, S.M. *Monopulse Radar Theory and Practice 2nd ed.*; Artech House, 2011.
15. Klein, L.A. *Millimeter-Wave and Infrared Multisensor Design and Signal Processing*; Artech House, 1997.